A Thesis Presented to

The Faculty of Alfred University

3D Motion Analysis from 2D Monochromatic Images of a Solar Prominence

Anthony David Gai

In Partial Fulfillment of

the Requirements for

The Alfred University Honors Program

May 8, 2013

Under the Supervision of:

Chair: Dr. Dave Toot

Committee Members:

Dr. David DeGraff

Dr. Allen Grove

Table of Contents

I. Acknowledgements

Funding for this project was provided by Gene and Pamela Bernstein, New York State NASA Space Grant Consortium, and the Rosing Summer Fellowship (Alfred University).

This project would not have been successful without the support and guidance from my advisor Dr. Dave Toot. His mentorship has directed me towards success over the past few years. His appreciation and passion for our nearest star has fueled my own ambitions toward the sun. Thank you to Dr. David De Graff for being an inspirational instructor and role model throughout my time at Alfred. To Dr. Grove, thank you for joining my committee and providing both a technical and outside perspective to the project.

To the technicians and directors at the Sacramento Peak facility, thank you very much for your hospitality and dedication.

II. Abstract

Solar prominences are the massive formations of ionized gas collecting above the Sun's surface. Even after more than half a century of research, there is not a full understanding of the processes involved in the formation, support, and features of solar prominences. Solar prominences are often associated with flares and coronal mass ejections, both of which can be harmful to the earth. A deeper understanding of these solar phenomena will protect us from dangerous solar storms. In this report I present 3D motion analysis, via Doppler measurements (H-α, H-β, and Na-D), extracted from 2D monochromatic images of a prominence observed on 10 October 2012 from the Richard B. Dunn Solar Vacuum Tower, Sacramento Peak, NM. Magnetograms from THEMIS, Tiede Observatory, Tenerife, Canary Islands, Spain describe the magnetic field. Monochromatic images from Hinode's Solar Optical Telescope provide high resolution views (Ca II and H-α).

III. Introduction

The Sun is a strong source of constantly changing magnetic fields. The ionized plasma is a rope in a constant tug-of-war match between changing magnetic fields and thermal pressures. Like most tug-of-war matches, they easily become violent. This leads to instabilities, often resulting in prominences, coronal mass ejections, and flares.

Prominences are some of the most spectacular features found on the Sun. The region above of the Sun's surface is called the corona. It is known for high temperatures (10^6 K) but low densities (10^7particles/m^3). Just inside lays the much smaller, much cooler (4400-10000K), but higher density (10^{12} particles/m^3 - Carroll/Ostile, 2007) chromosphere. Solar prominences describe any collection of material at chromospheric temperatures and densities collecting within the corona and are primarily visible in the Hydrogen-Alpha wavelength (Zirin, 1988). With all the gravity from the Sun, it was originally not understood how these formations suspended above the solar surface, but further study revealed that the Sun has trouble keeping prominences bounded. Magnetic tension is the largest contributor for supporting prominences (Hillier/Ballegooijen, 2013). Magnetic fields and gravity bind prominences, but a simple rule of thumb is that for any prominence that exceeds 50,000 km, the outward pressures will overpower the gravitational and magnetic chains in the tug-of-war match and will erupt outward within 48 hours (Zirin, 1988).

Prominences appear completely different when they are not seen in isolation outside the limb of the sun. Prominences appear bright against the cold background of space. However, when seen face on with the sun as the background, prominences appear dark or relatively cool. This formation is known as a filament even though it is just a prominence observed face on.

There are two main flavors of prominences: quiescent and active. Quiescent prominences are longer lived, sometimes lasting multiple solar rotations. They are found in and near active regions as well in quiet regions. Ascending prominences were once long-lived and have finally escaped the Sun's grasp. Physical support for prominences varies depending on the type of prominences, but the main contributors are hydrostatic and magnetic forces. The interactions governed by two sets of equations: Maxwell's Equations describing electric and magnetic fields and the hydrodynamic equations relating pressure, density, temperature, and flow (Zirin, 1988).

Active prominences are almost always associated with flares. Examples of active prominences are loops, coronal rain, surges, and sprays. Loops appear when material erupts from a single region and the plasma follows the binding magnetic field lines, bending the shockfront into a loop. Coronal rain is when prominence material forms higher in the corona and is pulled back down to the solar surface. Surges are "collimated ejected material previously not seen" (Zirin, 1988). Sprays are similar to surges, defined as "uncollimated ejecta previously visible as pre-flare elevated features" (Zirin, 1988).

Quiescent Prominences do not move much. In 1970, Liszka studied 100 prominences and only a few had velocities greater than 7 km/s. This is helpful because we can more accurately use Doppler measurements to find the movements of individual features within the prominence.

However, prominences can have rotational elements. Entire prominences can appear to twist. The situation may be further complicated as features within the prominence may also show rotational movement. Prominences are guided by magnetic fields and therefore it is not understood how these objects can rotate and twist without tightening and slowing as the magnetic field becomes more tightly wound. It's like twisting a rope; there is only a finite

amount of times one can twist a rope before it becomes more difficult to twist and begins to climb up on itself and kink.

Other phenomena worth noting are oscillations and magnetoacoustic/sonic waves. Large amplitude oscillations were first observed in 1969. Ground based observations found small amplitude oscillations (Harvey, 1970). These oscillations were attributed to either standing or propagating magnetohydrodynamic waves caused by the strong magnetic fields of the sun interacting with the solar plasma.

Different wavelengths of light look at different temperatures within the plasma. I narrowed my observations at the Richard B. Dunn Vacuum Tower down to three main wavelengths with strong emission at chromospheric temperatures: Hydrogen- Alpha (H-α), Hydrogen-Beta (H-β), and Sodium-D. The primary difference between each of these wavelengths is the optical depth. Observations at various optical depths provided details for the surface, interior structure, and beyond the prominence. Also, when a material moves the wavelength of emission changed via the Doppler Effect. In order for me to detail the movement of material within the prominence, Doppler shift measurements were recorded off of line center.

IV. Observations

A. Richard B. Dunn Vacuum Tower

The Richard B. Dunn Solar Vacuum Tower is located in Sunspot, NM. The tower extends 13 stories above Sacramento Peak and burrows another 67 meters into the rock. The telescope is equipped with an arsenal of instruments including a heliostat, Advanced Stokes Polarimeter, Diffraction-Limited Spectro-Polarimeter, CCD cameras, and a Universal Birefringent Filter (UBF) (NSO). At the Dunn Vacuum Tower the UBF was the main instrument used in this study. The UBF can filter down to a ¼ Angstrom band-pass at any wavelength of visible light, allowing observation of key lines in the solar spectrum. In this study the UBF was used to observe 11 different wavelengths, detailed in the following table.

Image In Sequence	Wavelength Name	Wavelength (nm)
1, 12, 23, 34, 45	H-β -0.5 Å	486.15
2, 13, 24, 35, 46	H-β Line-center	486.20
3, 14, 25, 36, 47	H-β +0.5 Å	486.25
4, 15, 26, 37, 48	Sodium-D -0.5 Å	588.95
5, 16, 27, 38, 49	Sodium-D Line-center	589.00
6, 17,28, 39, 50	Sodium-D +0.5 Å	589.05
7, 18, 29, 40, 51	H-α -1.0 Å	656.18
8, 19, 30, 41, 52	H-α -0.5 Å	656.23
9, 20, 31, 42, 53	H-α Line-center	656.28
10, 21, 32, 43, 54	H-α +0.5 Å	656.33
11, 22, 33, 44, 55	H-α +1.0 Å	656.38

Figure A: Above is the sequence of wavelengths measured.

Each data file was composed of 55 images, five from each of the 11 wavelengths. The UBF stepped through each wavelength from shortest to longest. The files were grouped into sets of five sequences in order to increase the amount of time observing (and decrease the "write time"). The time for the creation of the master file does not significantly vary if it is composed of 11 files or 55 files. Writing 55 files at once takes less time than stopping after each sequence to create a new log.

B. THEMIS

The Heliographic Telescope for Studying Magnetism and Solar Instabilities (THEMIS) is a French and Italian run solar telescope located on Mount Teide, Canary Islands, Spain. Construction began in 1993 and the telescope saw first light in 1996. The facility houses a 90 cm solar telescope for use in the measurement of intensity and direction of the solar magnetic field and high resolution imaging of the solar surface.

THEMIS provided us with a full vector field describing the magnetic field of the observed prominence. The full Stoke's profiles were provided in the Na I D3 line parallel to the limb.

C. Hinode

Hinode was launched in 2006 from Uchinoura Space Center, Japan. The satellite sits in helio-synchronous orbit at an altitude of around 600 km. That is, Hinode will always be on the day side of the Earth looking at the sun. The instrument used in this study is the Solar Optical Telescope (SOT). SOT is a 0.50 m telescope achieving a diffraction limited resolution of around 0.2 arc seconds, capable of observing fine structures in the photosphere and chromospheres (Hinode).

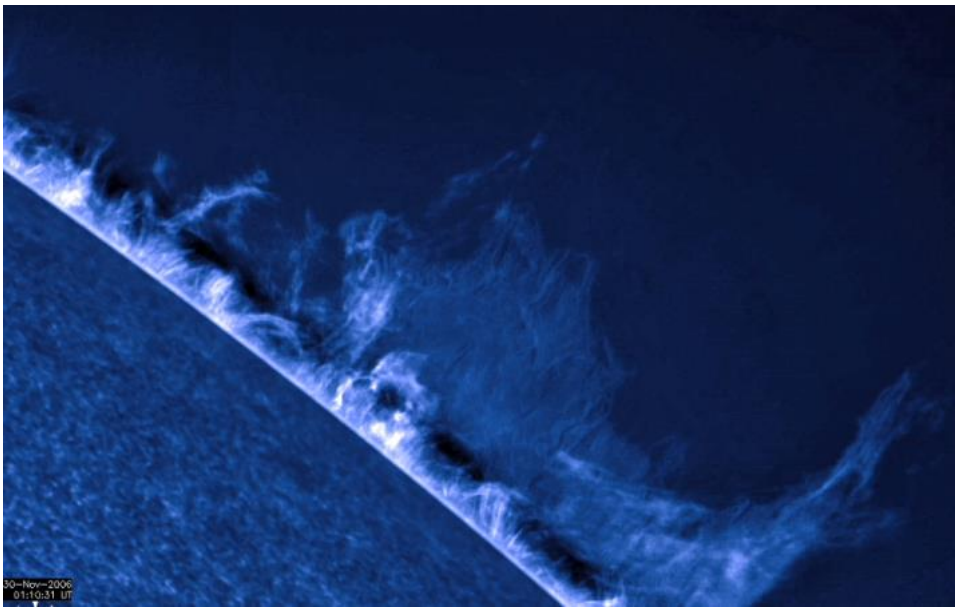

Figure B: The above image shows a quiescent prominence observed by Hinode's SOT at the wavelength for Ca II (389.6 nm) on November 30, 2006. Since Hinode is in space, the images are not affected by the turbulence and effects of the earth's atmosphere.

V. Data

The prominence was observed on the SW limb of the sun on 10 October 2012. The prominence seemed quiescent but showed signs of interaction with an active region located beyond the horizon of the sun.

Observations with the Richard B. Dunn Vacuum Tower were centralized around three wavelengths representing material at chromospheric temperatures (8000-10000K). In addition to the line-center observations, the Dunn Telescope observed in Doppler shifts off from line center. The Doppler shifts provided vital details about the line-of-sight motion of material within the prominence.

Images within the wings of the lines also revealed the structure of a wave phenomenon within the prominence. The wave was more clearly seen by subtracting Doppler shifts and therefore amplifying dominant motions.

The Hydrogen-Alpha line is Hydrogen's Balmer Alpha line. This wavelength of light occurs at 656.5 nm and represents an electron transition from the n=3 to the n=2 state. H-α is optically thick and helps us to see features on the “surface” of the prominence (Figure C).

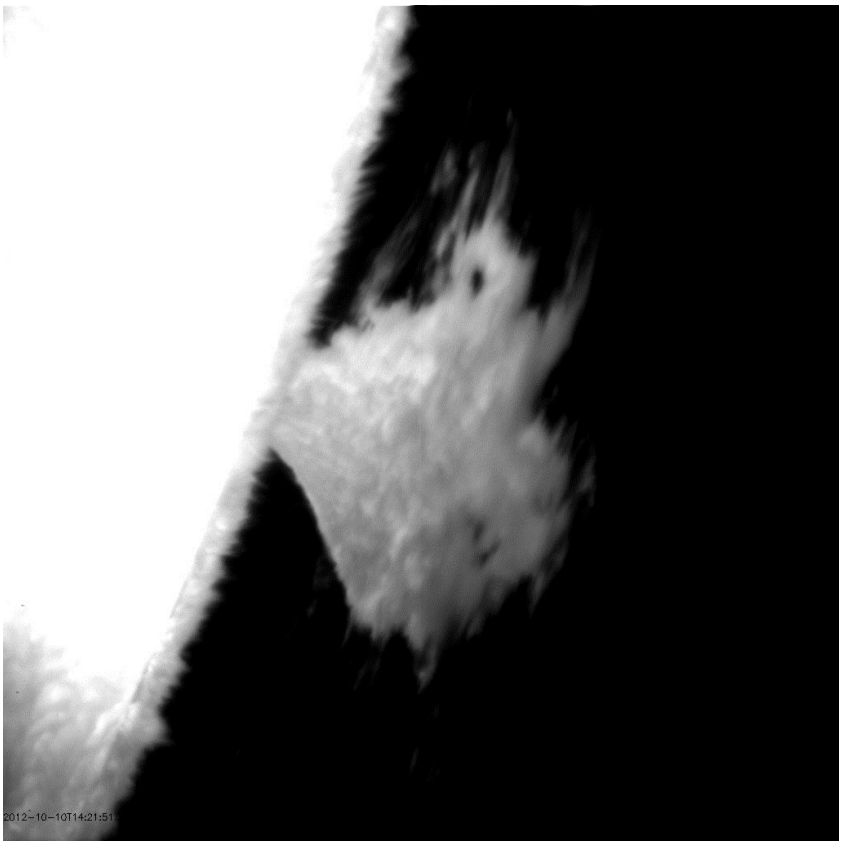

Figure C: The above image is an example of the observed prominence in H-α line center taken from Sacramento Peak, NM.

The Hydrogen-Beta line is the next jump in the Balmer series, describing an electron transition from the n=4 to n=2 state. The wavelength of H-β is 486.2 nm. H-β is optically thin, allowing us to see material and features within and behind the prominence (Figure D).

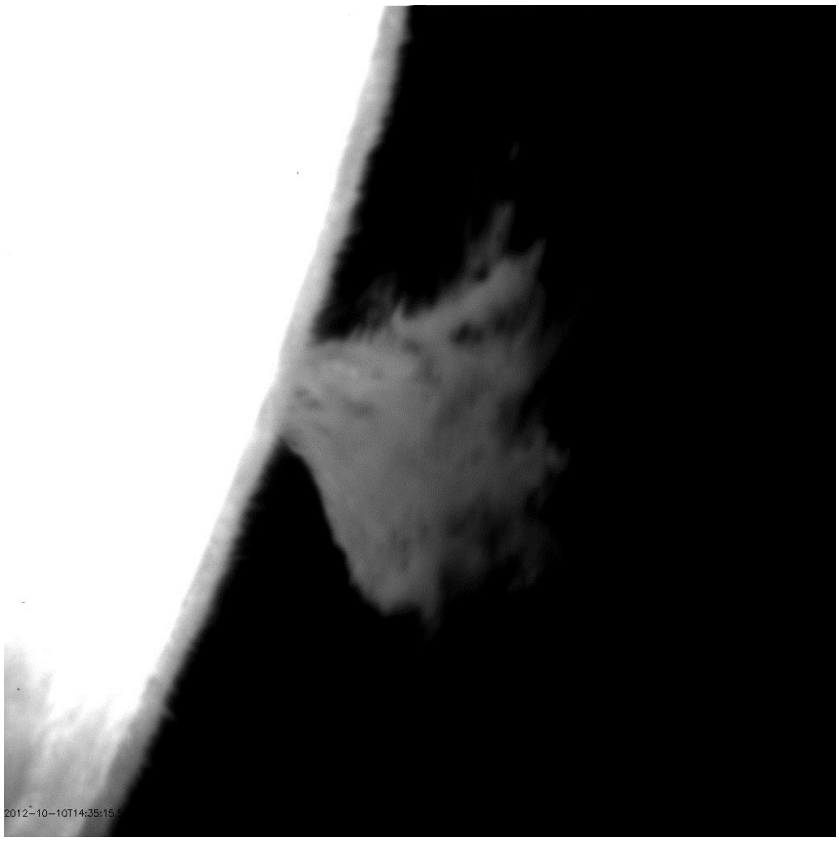

Figure D: This is an example image of the observed prominence in H-β line center from Sacramento Peak, NM.

Sodium-D occurs at 589.0 nm and is the most optically thin wavelength of the series (Figure E).

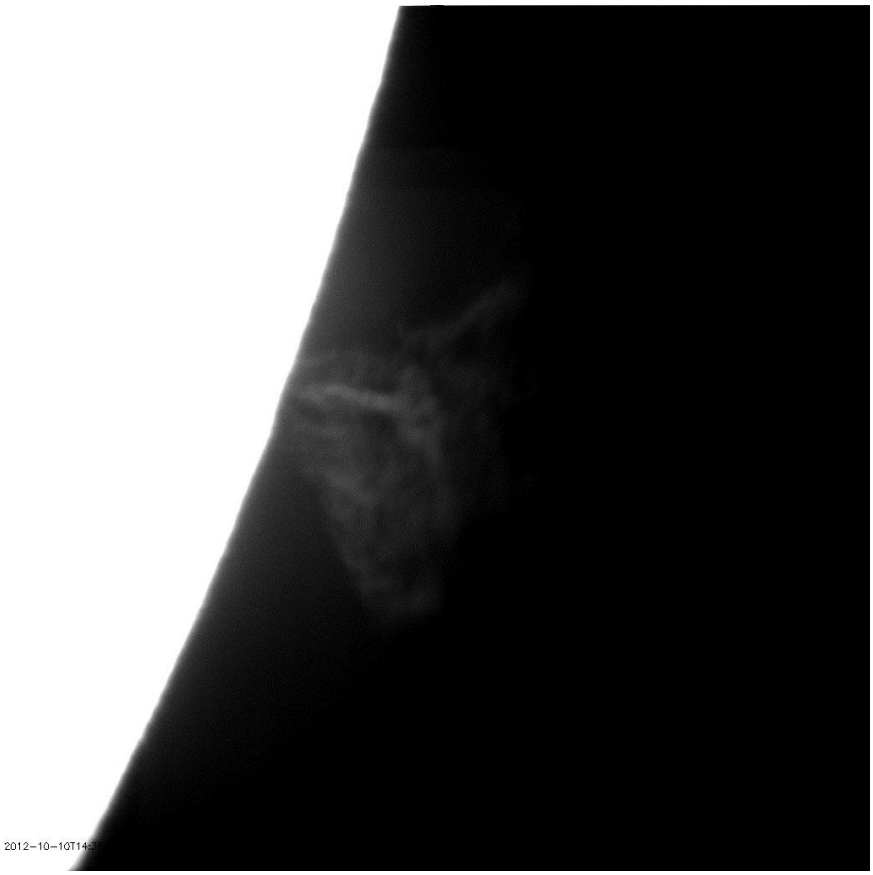

Figure E: This image was taken of the prominence in Sodium-D line center from, Sacramento Peak, NM.

VI. Analysis

A. Dopplergrams

Flats and darks were applied using IDL. Dopplergrams were created by subtracting images at opposite Doppler shifted wavelengths at each side of line-center in IDL. A dopplergram is an image that uses Doppler shifts to show the preferred motion of material. Material with no preferred movement appeared gray because there were just as many counts in the red-shift image as the blue-shift image. The Doppler images provided a range for the velocity of material in the line of sight axis.

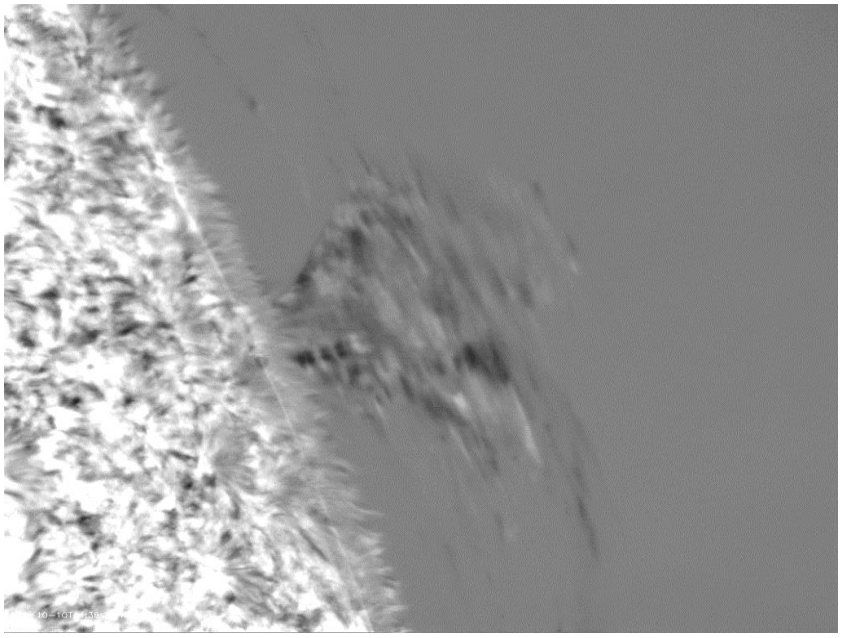

Figure F –H-α Dopplergram between +/- 0.5 Å images which represents material emitting in H-α moving at around 23 km/s. White represents blue-shifted or towards (-0.5 Å) and black represents red-shifted or away (+0.5 Å). Gray areas indicate no dominant line of sight motion.

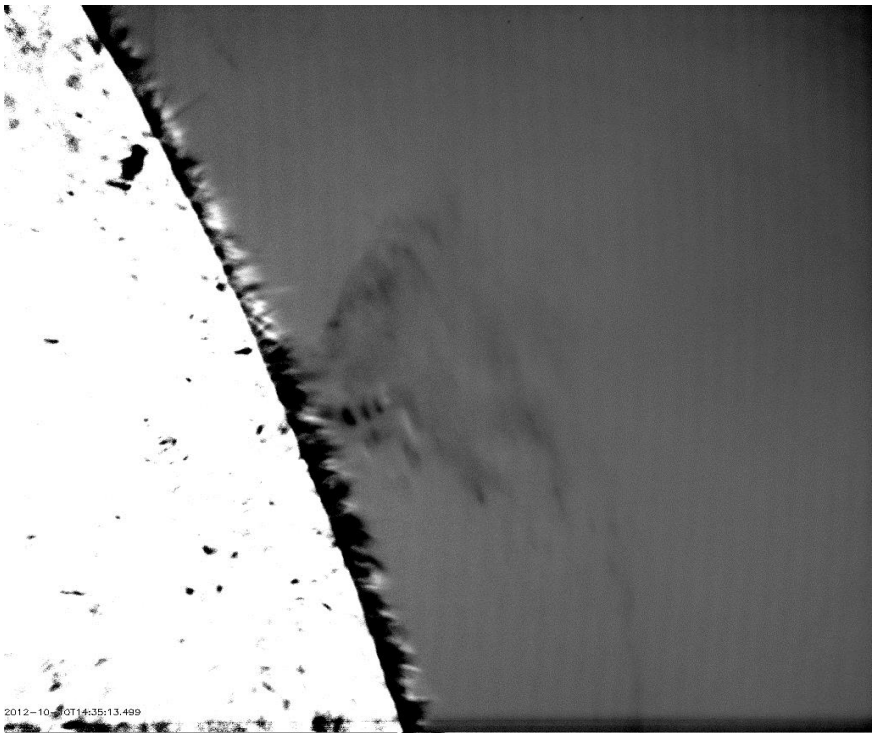

Figure G –H-β Dopplergram between +/- 0.5 Å images which represents material emitting in H-β moving at around 30 km/s. White represents blue-shifted or towards (-0.5 Å) and black represents red-shifted or away (+0.5 Å). Gray areas indicate no dominant line of sight motion.

B. Magnetoacoustic Wave

The Sac Peak images revealed a propagating wave within the core of the prominence. This can be seen in Figures F and G as the dark bands through the center of the prominence. Since the wave is observable in H-α (an optically thick wavelength), the feature must be occurring on the near side of the prominence. Later in the data set, the top of the wave appears to reverse direction and move back towards the surface of the sun. This is an indication the wave front does not have enough energy to escape the binding forces and falls back to the surface of

the sun or, more likely, the feature follows a projectile-like trajectory along our line of sight. This could be caused by the wave following a magnetic field supporting the prominence.

In the Dopplergrams the majority of the material does not have a preferred motion. The northern edge of the prominence tends to have a darker hue suggesting motion away. Likewise, the southern end tends to be lighter. Combined, this implies that the material has some sort of a rotational component. Prominences have been shown to have rotational elements before, but it is still not clear how this can occur without tangling the magnetic fields (Zirin, 1988). There is a possibility in the translational offset of the images which would result in the appearance of a rotational element; however, this would not explain the wavelike phenomenon in this study since the wave appears perpendicular to the potential offset in the images.

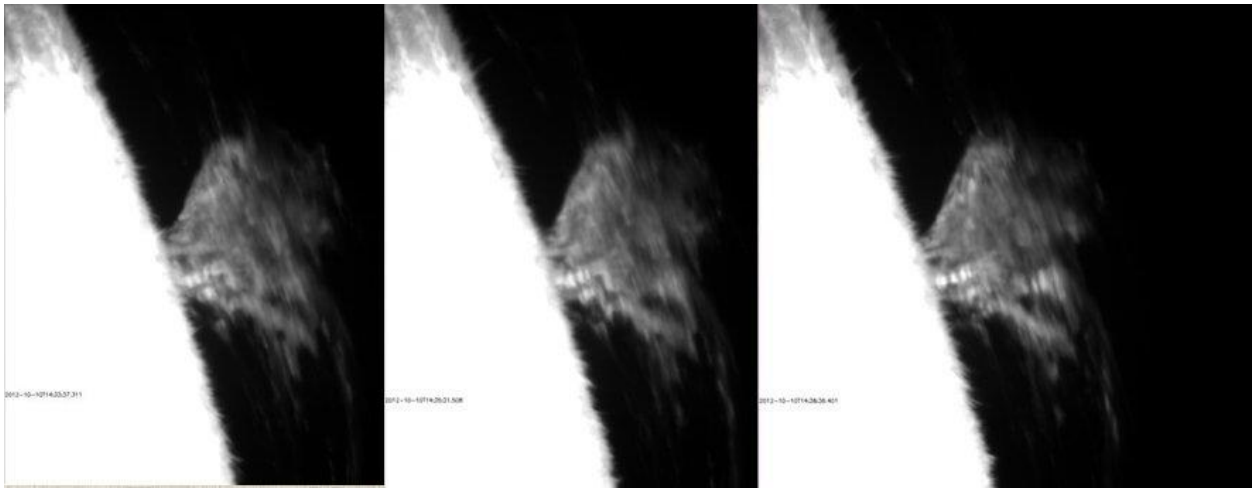

Figure H shows the prominence in line-center H-α at three times to show the progression of the wave observed in the prominence.

To measure the velocity of the wave, a cross-cut was taken through the center outputting counts per pixel. This showed where the maximum value occurred at each cycle and made it

possible to track a feature through time steps. This was done in H-β because the images showed the waves most distinctly.

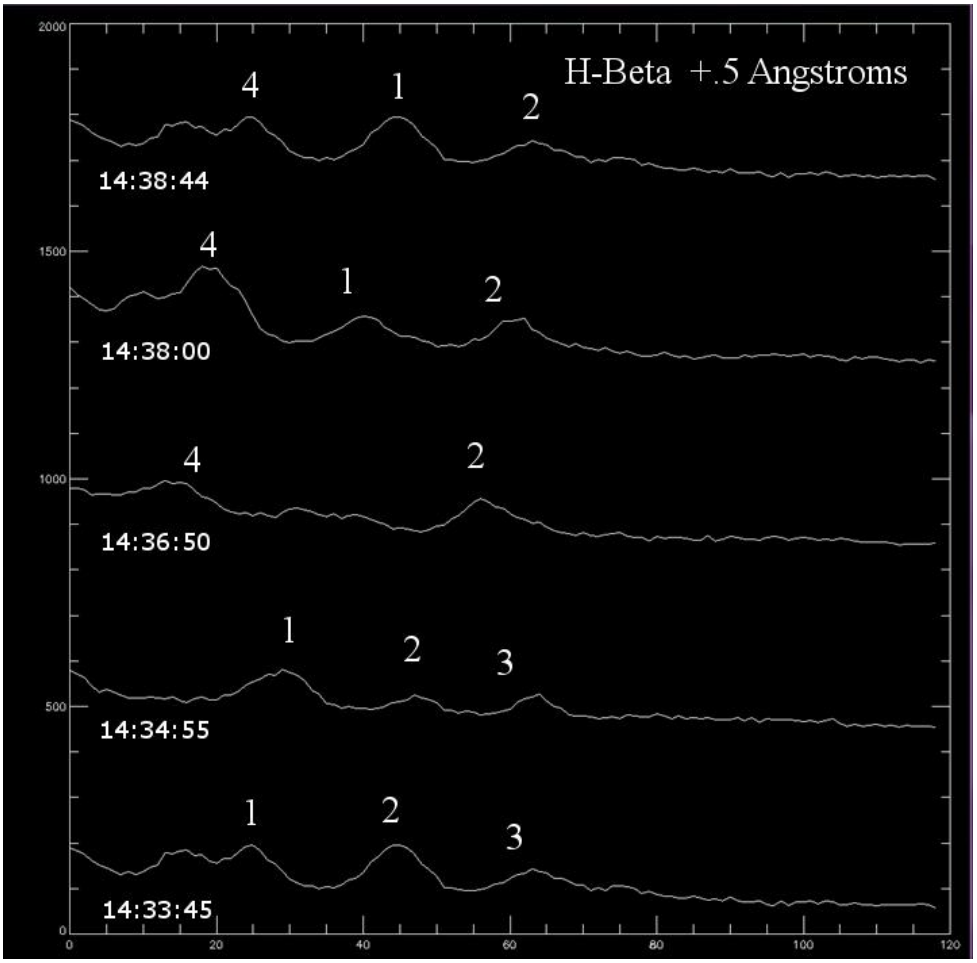

Figure I - The each cycle is numbered. Cuts begin at the limb of the sun and are plotted in sequential order with the earliest at the bottom.

The wave peaks all seem to move similar distances between images. This is evidence that there is one dominant wave propagating through. However, Wave Peak 1 dissipates at 14:36:50 but reappears just over a minute later. This could be an indication of other smaller waves, with different periods, causing interference. Another indication of a more complicated wave structure

is the size of each peak, which varies between time sequences. The table in Figure J describes the locations of the maximum value of each of the wave peaks along the cut. From the time between each image and the positions along each cut I determined the propagation speed.

H-β +0.5Å

Line #	Peak #1 (Pixel Location)	Peak #2 (Pixel Location)	Peak #3 (Pixel Location)	Peak #4 (Pixel Location)	Δ Peak #1	Δ Peak #2	Δ Peak #3	Δ Peak #4	Time (s)	V Peak #1 (km/s)	V Peak #2 (km/s)	V Peak #3 (km/s)	V Peak #4 (km/s)
1 (14:33:45)	25	44	63	-	-	-	-	-	110				
2 (14:34:55)	29	47	65	-	4	3	2	-	70	4.4	3.3	2.2	
3 (14:36:50)	-	56	-	15	-	9	-	-	115		15.4		
4 (14:38:00)	39	61	-	18	10*	5	-	3	70	10.4	5.2		5.1
5 (14:38:44)	43	63	-	23	4	2	-	5	44	10.9	3.4		13.6
									Averages	8.6	6.8		9.4

*Line 4 - Line 2

1 pixel = 120 km

Average	8.2 +/- 2 km/s

Figure J – A table showing the pixel number for each of the peaks and the corresponding velocity calculation.

Later in the data set, a second wave appears higher up in the prominence. An example image can be seen in the right picture of Figure C. However, upon analysis the wave did not protrude out from the background noise enough to be able to complete a cut analysis.

C. Alfvén Speed

THEMIS measurements in the Na-D line describe a fairly uniform magnetic field of around 0.001 T. This is average for prominences (Schmieder, 2012).

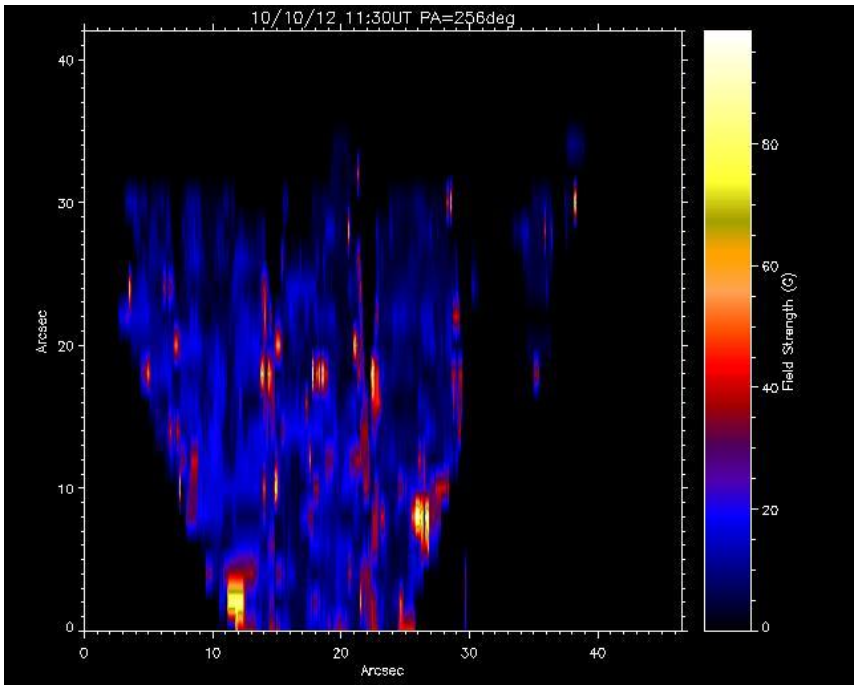

Figure K details the strength of the **B** field throughout the prominence. Schmieder noted that the peaks are most likely errors in the inversion and are not real.

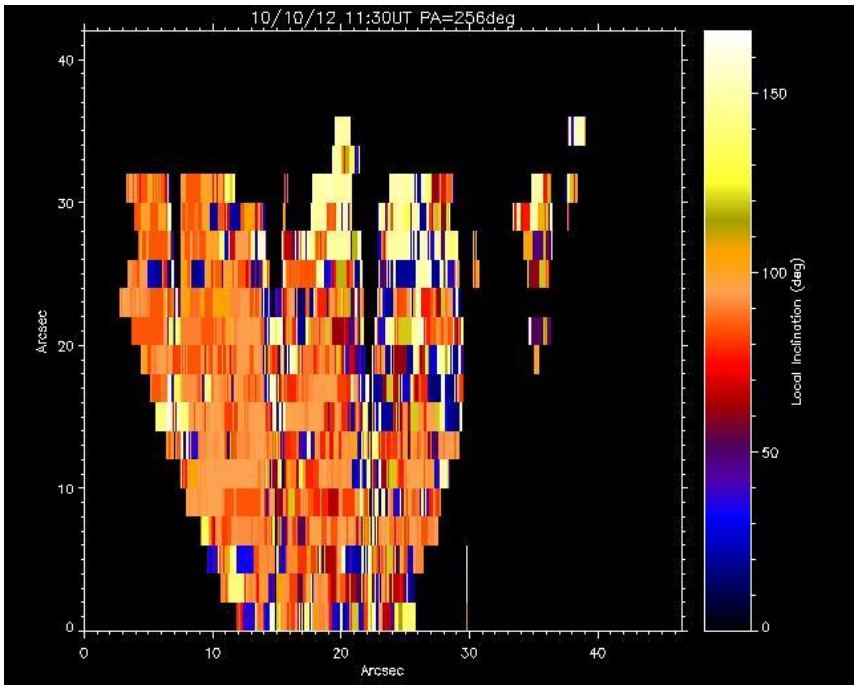

Figure L shows the angle at which the **B** field is oriented. 180° means vertical while 90° means horizontal.

The Alfvén speed is defined by the following equation.

$$V\boldsymbol{a} = \frac{\boldsymbol{B}}{\sqrt{2\mu_{\circ}\rho}}$$

With the chromospheric physical densities described by Carroll and Ostile and the magnetic field measurement we can estimate the Alfvén speed within the region, resulting in an Alfvén speed of 14 km/s.

D. Error Analysis

The translational waves have an error margin of 2 km/s. The Doppler measurements, using a $\Delta\lambda$=0.25 Å, correspond to an error margin of 10 km/s. The total error is dominated by the error in the Doppler measurement giving us a total error of +/- 10 km/s.

VII. Conclusion

Analysis of the wave peaks resulted in a wave propagation of 8 +/- 2 km/s. This is within an order of magnitude estimation of the Alfvén speed. This result is in agreement with an analysis done on Hinode observations of the same prominence (Knizhnik, Kalman. 2013). Because of the direction and orientation of the magnetic field and the velocity at which the wave propagates, we believe the wave is magnetoacoustic. Doppler measurements combined with the wave propagation describe the material moving within a range of about 31 +/- 10 km/s.

The wave pulses seem to appear and disappear, which could be an indication of interference between waves of different frequencies.

Future work should entail an analysis of high resolution Hinode data to more accurately determine the speeds of material within the prominence. More rigorous comparisons and analysis of Themis magnetogram data will help refine the estimation on the Alfvén speed within the region. Fourier analysis on the waves could provide details underlying the driving methods. 3D plots could be rendered from the supplied information.

VIII. References

Carroll, Bradley W., and Dale A. Ostlie. *An Introduction to Modern Astrophysics*. San Francisco: Pearson Addison-Wesley, 2007. Print.

Harvey, J. W. "Short Period Oscillations and Doppler Velocity Gradients." *Solar Physics* 11.1 (1970): 26-28. Print.

Hillier, Andrew, and Adriaan van Ballegooijen. “On the Support of Solar Prominence Material by the Dips of a Coronal Flux Tube.” *Astrophysical Journal*. 18 March 2013: Print.

Knizhnik, Kalman. Personal Communication. 2013

Liszka, Ludwik. "Measurements of Line-of-sight Velocities in Prominences." *Solar Physics* 14.2 (1970): Print.

"National Aeronautics and Space Administration." *Hinode (Solar-B)*. NASA, Web. 06 May 2013.

"Richard B. Dunn Solar Telescope." *Welcome to Sacramento Peak*. National Solar Observatory, Web. 25 Apr. 2013.

Schmieder, Brigitte. Personal Communication. 2012-2013.

"THEMIS." *Instituto De Astrofisica De Canarias*. Web. 25 Apr. 2013.

Zirin, Harold. *Astrophysics of the Sun*. Cambridge, 1988. Print.